Microsyst Technol (2013) 19:1005–1015
DOI 10.1007/s00542-012-1691-x

TECHNICAL PAPER

MEMS tri-axial force sensor with an integrated mechanical stopper for guidewire applications

Woo-Tae Park · Rama Krishna Kotlanka · Liang Lou · Muhammad Hamidullah · Chengkuo Lee

Received: 17 June 2012 / Accepted: 17 October 2012 / Published online: 3 November 2012
© Springer-Verlag Berlin Heidelberg 2012

Abstract This paper describes the design and characterization of a micro-electro-mechanical systems tri-axial force sensor that can be mounted on the tip of an 1-French guidewire (0.014″). Piezoresistive silicon nanowires (SiNWs) are embedded into four beams forming a cross-shape to allow the detection of forces in three axes. The electrical resistance changes in the four SiNWs are used to decode arbitrary force applied onto the force sensor. Finite element analysis was used in the structural design of the force sensor. Robustness of the force sensor is improved due to the novel design of incorporating a mechanical stopper on the tip of the stylus. Flip chip bonding, using gold stud bumps, is used to mount the force sensor on a substrate for characterization and to simplify the assembly process. The sensor is robust enough to withstand normal forces higher than 20 gf. The proposed sensor can be used for new medical applications in vascular interventions and robotic surgeries.

W-T Park and R. Krishna Kotlanka contributed equally as first author.

W.-T. Park · R. K. Kotlanka · L. Lou · M. Hamidullah · C. Lee
Institute of Microelectronics, A-STAR, 11 Science Park Road, Singapore 117685, Singapore

W.-T. Park (✉)
Department of Mechanical and Automotive Engineering, Seoul National University of Science and Technology, Seoul 135-743, Korea
e-mail: wtpark@seoultech.ac.kr

R. K. Kotlanka
Engineering Product Development, Singapore University of Technology and Design, Singapore 138682, Singapore

L. Lou · C. Lee
Department of Electrical and Computer Engineering, National University of Singapore, Singapore 117576, Singapore

1 Introduction

Advances in surgical tools and their associated techniques advocate implementation of minimally invasive surgery (MIS). For MIS in cardio-vascular and thoracic interventional procedures, passing a guidewire through vascular vessel is the first step followed by the surgical procedures such as stenting. The ability to successfully treat a vascular lesion via endovascular methods is dependent on the ability to pass a guidewire across the lesion. Blockage of the vessel lumen in the range from 50 to 100 % makes passage of the guidewire a challenging task.

Passage of the guidewire is primarily through the haptic feeling of the surgeon (accompanied with eye–hand coordination for on screen X-ray imaging) and the force feedback of the passing guidewire is extremely difficult to quantify. Quantitative information of force feedback of the passing guidewire can be used in assisting the surgeon with more information, facilitating robotic aided surgeries, and training the residents in the future. A conceptual drawing of a guidewire with the tactile sensor tip is shown in Fig. 1.

Microelectromechanical systems (MEMS) enabled the possibility of making sensorized guidewires and catheters for identifying and analyzing the stenosis without excessively using intravenous contrasts (Rebello 2004; Bonanomi et al. 2003; Tonino et al. 2009; Takizawa et al. 1999). MEMS sensors were first used to identify stenosis. Rebello (2004) reported that there is a change in temperature (approximately 3 °C) at the location of the stenosis, thus recommending the use of temperature sensor at the tip of the guidewire. Bonanomi et al. (2003) mentioned that force sensors can be used for identifying the stenosized location by obtaining the hardness information of the tissue. This is because the hardness of the calcified tissue at stenosis location is higher than the healthy vascular vessel. Once

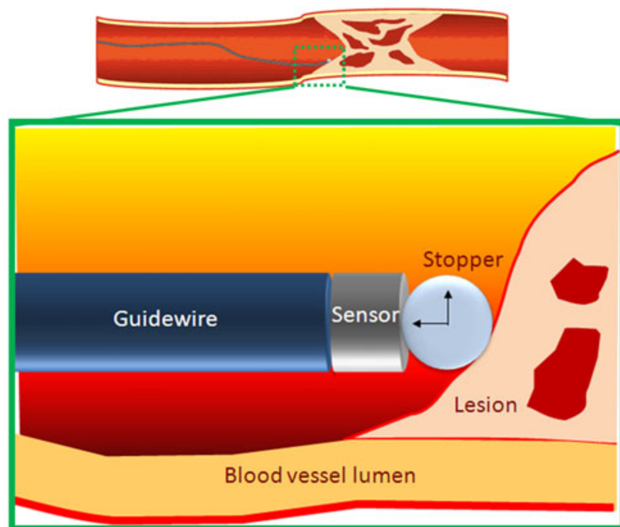

Fig. 1 Close up conceptual view of the guidewire with tactile sensor tip inside the blood vessel in contact with a vascular lesion

the stenosis is found, the degree of stenosis is important. Tonino et al. (2009) reported placing a pressure sensor near the tip of the guidewire and measuring fractional flow reserve (FFR, ratio of pressure before and after stenosis) to get the information of the blockage degree, can reduce the rate of composite re-stenosis symptoms and other complications.

Tactile sensing was also used for cardio-vascular MIS. To obtain the contact information of the catheter while making a touch to the vascular vessel, Takizawa et al. (1999) reported the assembly of three pressure sensors at an angle of 45° on the axis of the catheter. Tri-axial force sensor on the surgical scalpel for obtaining force applied by the surgeon for making incisions was demonstrated by Valdastri et al. (2006, 2007). Neuzil et al. (2010a) reported using a tactile sensor catheter to assess the contact force during radio frequency (RF) ablation, so sufficient force can be applied during the ablation procedure to reduce recurrence.

In MEMS force sensor area, four beam design is the most prominent (Fahlbusch et al. 1998; Beccai et al. 2005; Tibrewala et al. 2008; Jin and Mote 1998) as it allows force sensing in all the three axes with a relatively simple structure. For this design, piezoresistive transduction method is the most appropriate for implementing for force sensing. For all these sensors, robustness of the sensor was improved through packaging techniques making the whole system much bigger though the miniaturized sensor was used. Capacitive sensing tri-axial force sensors were also reported to show excellent resolution (Beyeler et al. 2009). Capacitive sensing generally requires signal conditioning to be close, because of the influence of parasitic capacitance in long connections. Piezoelectric force sensors can be used as well but have limitation in static changes.

In this paper, we report a piezoresistive tri-axial force sensor using a four beam design, with integrated force mechanical stopper to enable robust operation, small foot print, and simpler assembly process. We are proposing such tri-axial force sensor to be used for the sensorized guidewire application to sense tri-axial reacting force on contact, and to be used to assess the hardness of the contacting tissue.

2 Sensor design

2.1 Piezoresistive transduction and silicon nanowire piezoresistors

Piezoresistive transduction has been widely used in MEMS sensors since the first report by Smith (1954). The sensing mechanism of piezoresistive sensors lies in silicon's ability to change carrier mobility under strain, which is at least an order of magnitude higher than the resistance change by geometric effect. The proportional change in electrical resistance can then be measured commonly using a Wheatstone bridge. When resistance change can be expressed in terms of piezoresistive coefficient and stress as below,

$$\Delta R/_R = \pi_l \sigma_l + \pi_t \sigma_t \quad (1)$$

($R \equiv$ resistance, $\pi \equiv$ piezoresistive coefficient, $\sigma \equiv$ stress, l and t subscripts refer to longitudinal and transversal components).

Gauge factor (GF) is the measure of sensitivity of a strain sensor, and defined as below (Eqs. 2 and 3). As can be seen from the equation, for a given strain, the sensor response amount (resistance change) will depend on the GF.

$$\varepsilon * GF = \frac{\Delta R}{R} \quad (2)$$

$F \equiv$ gauge factor, $R \equiv$ resistance, $\varepsilon \equiv$ strain).

Longitudinal component is defined by having stress and current in the same direction, and transversal component is defined as orthogonal direction to each other. Neuzil et al. (2010b) reported that piezoresistive effect of SiNW has been shown to be increasable up to GFs of 5,000 from 50 in bulk by shrinking cross-sectional dimensions and applying back-gate bias voltage. The physics behind this enhancement has been explained based on a stress induced shift of the surface Fermi level in depleted structures (Rowe 2008). Neuzil also reported the GF is similar to bulk value at zero bias, but gets the giant factor by the back-gate bias. In this paper, because of the complexity and stringent measurement conditions required by the high GF with back-gate bias, we chose to use 'no-bias' condition. This simplifies the connections and makes the sensor signal output more robust from noise. We still use silicon nanowire for the

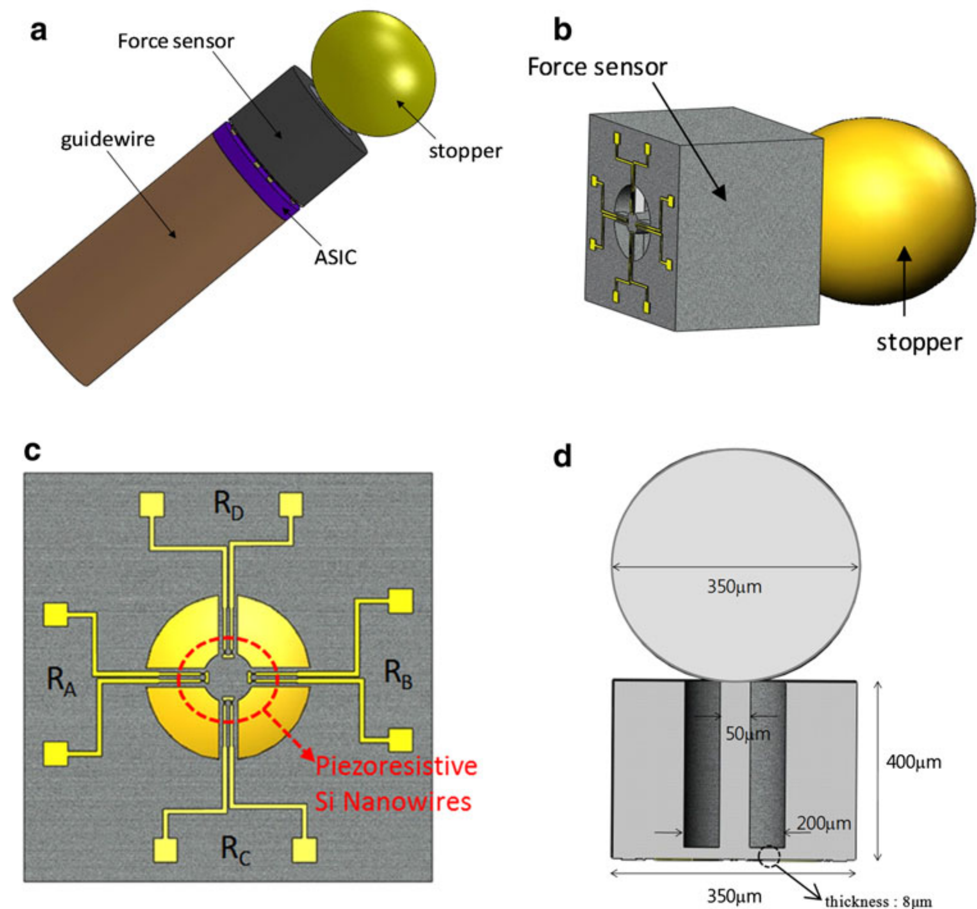

Fig. 2 **a** Schematic of force sensor on a guidewire, **b** three dimension details of the MEMS structural features, **c** piezoresistive Si nanowire location within the crossbeams, **d** *cross-sectional schematic* showing the vertical Si beam connecting the cross-beams and the mechanical stopper

sensing element at no-bias condition but can adopt biased condition for future applications that require higher GF in a more controlled environment.

2.2 Tri-axial force sensor design

Wide ranges of guidewires are available and the most commonly preferred guidewires are <0.36 mm (exactly 0.014″) in diameter (Asahi Intecc 2010). In order to facilitate feedback of the contact forces that the guidewire will make with the vascular vessel, a triaxial force sensor is proposed to be placed at the tip of the guidewire. Schematic of the sensorized guidewire is shown in Fig. 2a. The MEMS force sensor is flip chip bonded at the tip of the guidewire assembly. As typical guidewire assembly, final assembly will require some level of manual assembly. In this paper we will concentrate on the MEMS sensor while integrating MEMS and ASIC onto the guidewire is an ongoing research. 3D drawing of proposed tri-axial force sensor with integrated mechanical stopper is shown in Fig. 2b. The force sensor is square shape from the wafer dicing, which in later assembly need coating to make it round as the guidewire shape. The cross beam sensing element of force sensor is at the bottom of the sensor. The stopper is attached at the top side of the sensor. Figure 2c shows the plan view of the bottom of the force sensor. There are four piezoresistive silicon nanowire resistors embedded on the surface of the four beams forming a cross shape. For the flexible structure, cross-beam design comprised of four beams instead of using a full membrane has previously been reported and shown to be much more sensitive (Tibrewala et al. 2008). The vertical silicon rod at the center of the force sensor is connected between the mechanical stopper and the four cross beams as shown in Fig. 2d. It acts as a lever arm in transferring the forces that comes onto the mechanical stopper to the four beams. The deformations on the four beams allow the measurement of a tri-axial force as the strain distribution due to forces along the three different axes. The relation of the applied force to strain response of the force sensor to normal and tangential force loadings can be written as the following (Jin and Mote 1998):

$$\begin{bmatrix} F_x \\ F_y \\ F_z \end{bmatrix} = \begin{bmatrix} (\phi_t)/2 & 0 & -(\phi_t)/2 & 0 \\ 0 & (\phi_t)/2 & 0 & -(\phi_t)/2 \\ (\phi_n)/2 & 0 & (\phi_n)/2 & 0 \end{bmatrix} \cdot \begin{bmatrix} \varepsilon_1 \\ \varepsilon_2 \\ \varepsilon_3 \\ \varepsilon_4 \end{bmatrix} \tag{3}$$

where,

$$\emptyset_n = \frac{4Ebt^3}{3(1-2x)h_0},$$

$$\emptyset_t = 1/\left(\frac{6h_0 d}{Ebt^3(1+\alpha_{km})}\left(1-\frac{3x}{l}\right)+\frac{1}{2Ebt^3(1+\alpha_{kf})}\right),$$

$$\alpha_{kf} = \frac{4b^2}{l^2}, \alpha_{km} = \frac{t^2}{8b^2(1+v)}$$

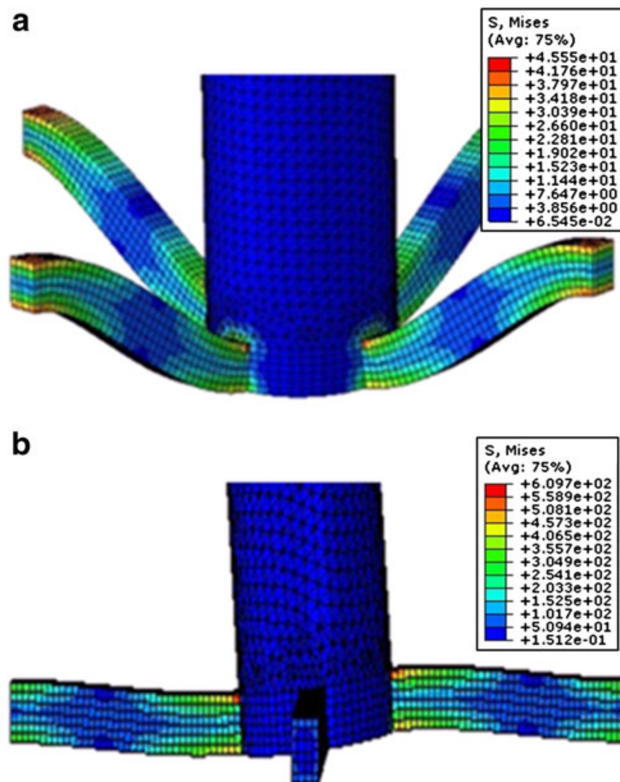

Fig. 3 ABAQUS™ simulation of silicon beam strain on **a** normal and **b** tangential loading of 10 mN at the tip of the pillar (cylinder) of the sensor

F_x, F_y, F_z are the force components applied to the sensor, ε_1, ε_2, ε_3, ε_4 are the silicon nanowire strain change in the four cantilevers respectively. h_o is the distance from the SiNW to the neutral axis, l, b and t are the beam length, width and thickness, respectively. x is the silicon nanowire sensor position, and is measured from the beam end at the support. d is the distance from the neutral axis of the beam to the tip of the pillar, E is the material's Young's modulus, and v is the Poisson's ratio.

ABAQUS™ was used to simulate the deformation of the beams at 10 mN of normal and tangential force. The beam length (75 μm) dimension was selected by the constraint of guidewire size and flip chip bond pads, and the rest of the dimensions (pillar diameter 50 μm, pillar length 400 μm, beam width 8 μm, beam thickness 12 μm) were selected by fabrication limits. Beam thickness selection will be discussed in the stopper analysis. The simulation was used to display only in-plane strain components. From the results, it is apparent that during normal loading, the lateral strain components in the four beams are equal in magnitude and in the same direction (Fig. 3a). When a tangential load was applied, the piezoresistors situated on each side of the rod (orientated along the force) experience strain in the opposite direction enabling differential sensing. The piezoresistors oriented orthogonal to the tangential force, experience torsional force that will not affect the piezoresistors (Fig. 3b). The simulated response also matches the theoretical equations (Eq. 3).

A comprehensive study was carried out on the size effects of the stopper. The function of the mechanical stopper is to protect the cross-beams from breaking due to excessive displacement coming from the ambient force while passing the guidewire. While the guidewire is passed through the vascular vessel, the spherical mechanical stopper provides smooth contact to the vascular vessel and at the same time translates the force onto crossbeams

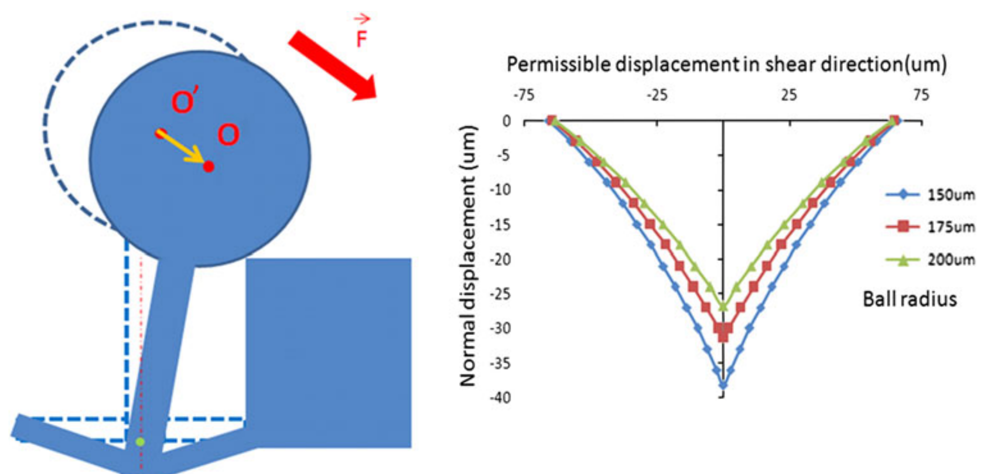

Fig. 4 Permissible displacement depending on the stopper ball size. The smaller the stopper, the higher force and displacement range. Both normal and shear direction displacement can be applied simultaneously

through the connecting rod. Due to the spherical shape of the mechanical stopper, there will be a limited permissible displacement for the cross beams as the stopper will touch the periphery of the silicon. Due to the stopper, the cross-beams are safe for excessive force while the stopper itself gets compressed. The permissible displacement in the normal and shear direction was calculated relating to the stopper ball size (Fig. 4). The relation was derived based on trigonometry. As the stopper ball size increases, the permissible displacement reduces. Since the movement of the stopper will most likely have normal and transverse component simultaneously, both displacement component are calculated together. In order to reduce the amount of displacement, larger stopper size needs to be used. Using

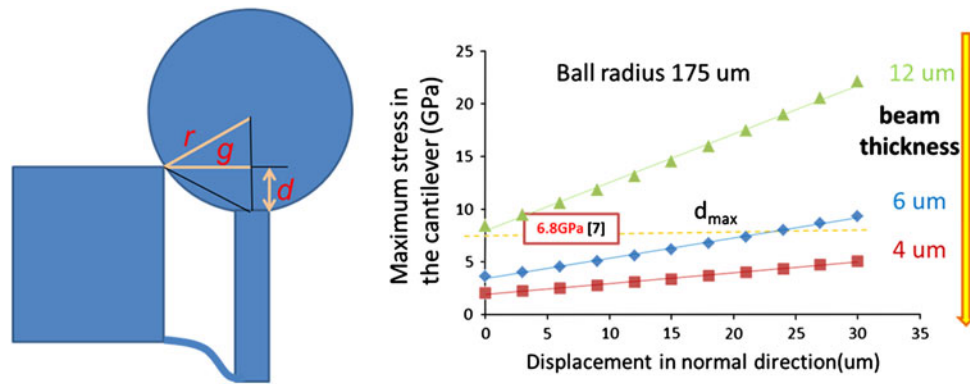

Fig. 5 Stopper ball size selection depending on beam thickness. From Eq. 4, the allowable displacement is calculated, and from ABAQUS™ simulation, the maximum stress in the cantilever is simulated for each beam thickness and normal displacement. Finally stopper ball size can be recommended based on the maximum stress allowed by Petersen (1998) and desired normal displacement range for the given beam thickness

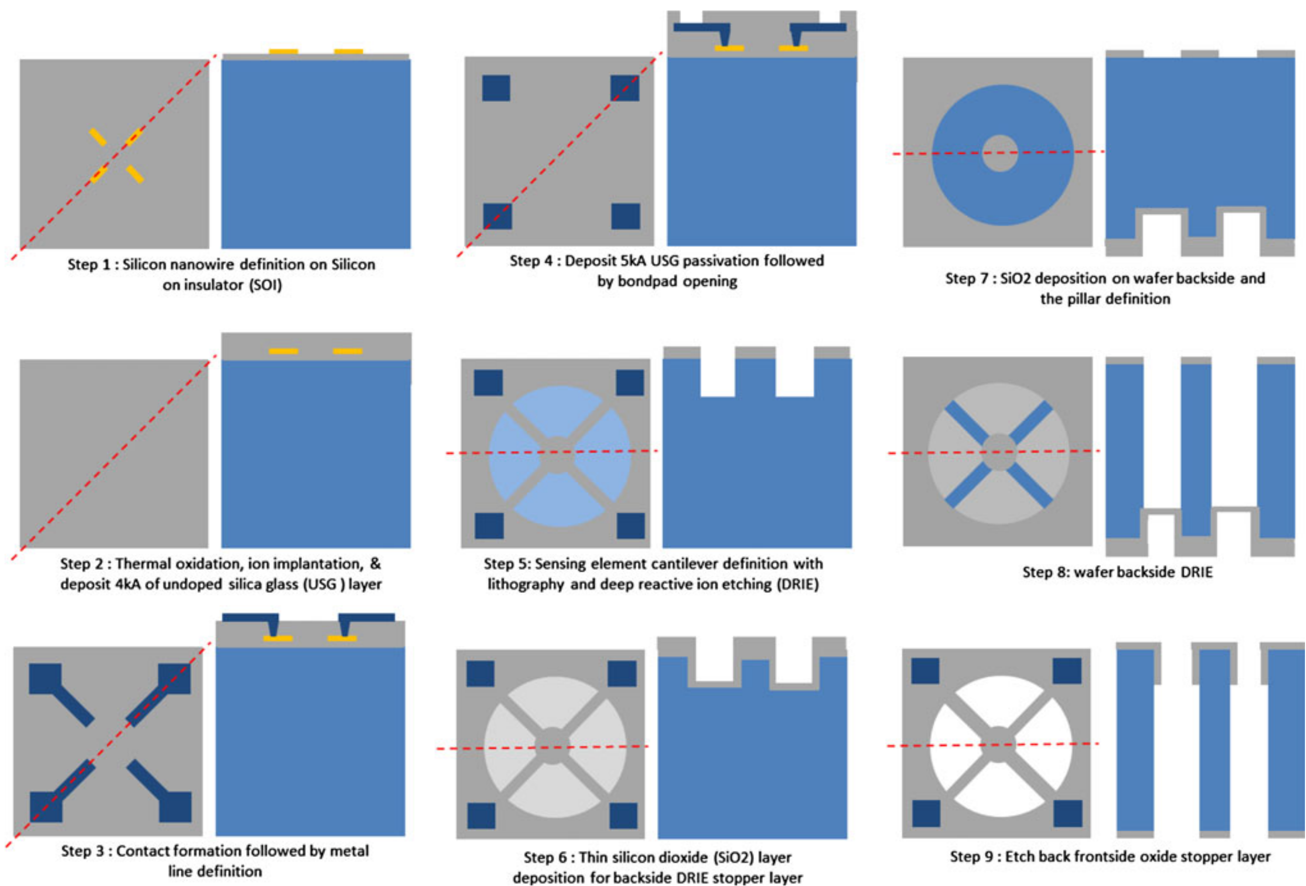

Fig. 6 Fabrication steps of tri-axial force sensor

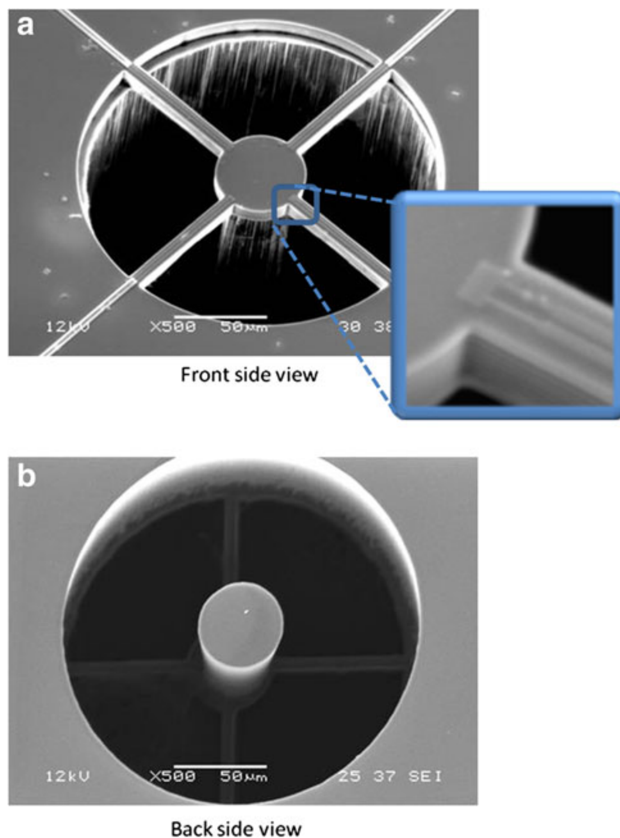

Fig. 7 SEM images of finished force sensor from **a** *front side* showing the silicon piezoresistor in the *magnified view*, and **b** from the *back side* from the rod

ABAQUS™, the maximum stress in the beam was calculated depending on the beam thickness and the normal direction displacement (Eq. 4, Fig. 5). For a beam thickness of 6 µm, the minimum stopper ball radius size need to be over 285 µm to be safely under the fracture stress reported previously (Petersen 1998).

$$d_{allow} = r - \sqrt{r^2 - g^2} \le d_{\max}, r \ge \frac{d_{\max}^2 + g^2}{2d_{\max}} \quad (4)$$

(where r = radius of stopper ball, g = length of beam, d_{allow} = displacement allowed from Fig. 4).

This graph shows the functionality of the stopper. The displacement in the cross beam increases until the stopper makes contact on the substrate rim. Further increased force on the stopper does not increase the displacement on the cross beam. This insures that the cross beam is protected from excessive force from the stopper.

3 Fabrication

The fabrication flow of the force sensor is shown in Fig. 7. Fabrication of the force sensor starts with an 8-inch SOI (silicon on insulator) wafer with 1,170 Å silicon device layer, 1,450 Å buried oxide layer, and 725 µm handle silicon. The nanowire piezoresistors were created by standard scanner lithography (Nikon KrF DUV Lithography), further resist-trimming using plasma etch, and finally trimming oxidation (O_2, 875°C, 2 h). The resulting nanowire piezoresistor cross section dimension was 70 × 70 nm, and 1 µm in length. Next, ion implantation was used to dope the piezoresistors and conductive regions separately in two steps. The resulting doping level of the piezoresistors was 1E14 (Boron) with 1,600Ω/4 kÅ of undoped silica glass (USG) layer was deposited, patterned and etched, to be used as the isolation layer between the resistors and the metal connection. After metal (aluminum) layer was deposited,

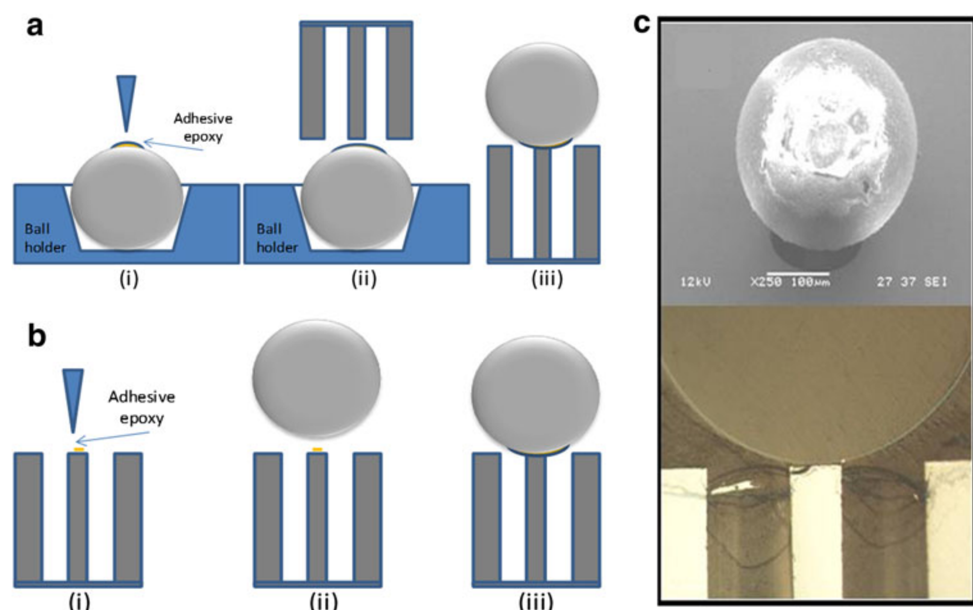

Fig. 8 Assembly process for stopper attachment using **a** flip chip bonding, and **b** manual attachment. Images from finished devices are shown in **c**

patterned and etched, another 5 kA of USG layer was used to passivate the metal layer. After the passivation layer was patterned to reveal the bondpads, the beam was defined and etched by deep reactive ion etching (DRIE). Another 1 kA of USG was deposited to preserve the beam from the subsequent backside etch. Next, the wafer was grinded and polished to a thickness of 400 μm, which is, in our experience, a thickness that is sturdy enough to be handled by standard semiconductor equipment for 8-inch wafers. Backside of the wafer was now deposited of 1 μm USG, and then patterned and etched by the backside etch mask. After 1 um oxide etch, backside was etched by DRIE until frontside etch patterns could be seen from the backside. Final beam thickness is 8 μm. Wafer was finally flipped back to the front side to remove the 1 kA protective USG by plasma etching of oxide. Scanning electron microscope (SEM) images of the finished force sensors are shown in Fig. 7.

After the force sensor was formed, the next step was to bond with the ball mechanical stopper. Originally, solder ball was proposed to be used as stopper material by depositing Cu–Sn on the silicon rod, and create solder eutectic bonding by flip-chip technique. However, due to biomedical application of this device, biocompatibility of the used material is of the utmost importance. Thus polystyrene beads were used to replace the solder balls. Polystyrene beads from Polysciences, Inc. were used with diameter of 350 μm. Adhesive epoxy from Inmat Technologies was used to create bonding between silicon rod and polystyrene bead with curing temperature of 150°C in 60 s. Figure 8a summarized the stopper attachment process using flip chip bonding method. The flip-chip process temperature was set at 150 °C, with 60 s bonding time for the purpose of epoxy curing. Polymer stopper was placed on the holder and adhesive epoxy was dispensed on the top of the polymer ball. Micromanipulator was used with probe tip size 1.5 μm to dispense small amount of epoxy on the silicon rod for precise positioning. Silicon rod was aligned and bonded using flip-chip equipment Suss Microtec FC150. No additional curing was needed because the flip-chip temperature and time were enough to cure the epoxy. Minimum contact force of 5 gf was applied, as the equipment was not stable and consistent load below 5 gf.

As it is not possible to reduce the flip-chip contact force, manual direct placement of polystyrene bead on the silicon rod was done as described in Fig. 8b. Using the same micromanipulator and probe tip, epoxy is dispensed on the silicon rod, and then manually dropped polystyrene bead on the silicon rod. By this method, the load applied was assumed to be zero and oven curing is used to cure the epoxy. The alignment was a concern for this method, but samples with acceptable alignment have been successfully fabricated. Images from finished stopper attachment SEM and cross section are shown in Fig. 8c.

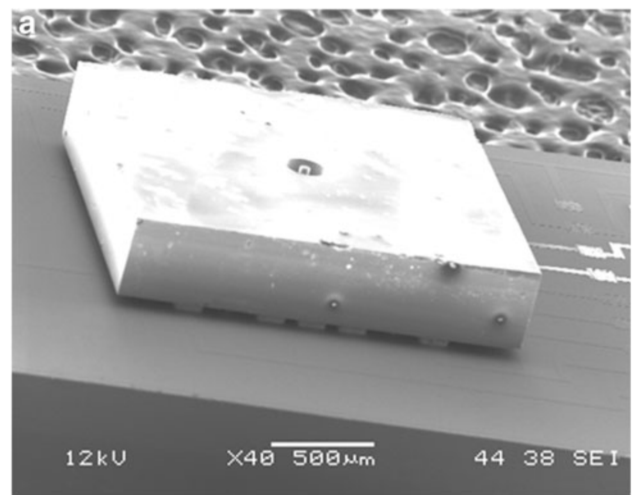

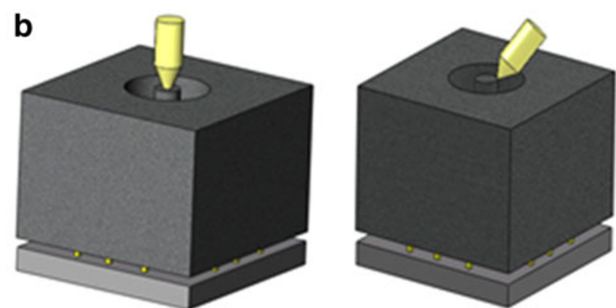

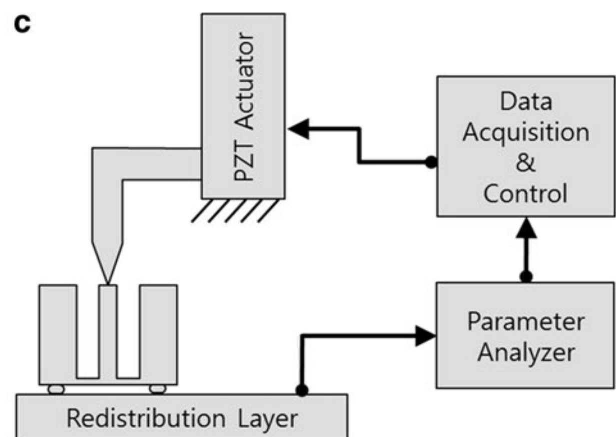

Fig. 9 **a** SEM of force sensor shown flip chip bonded to characterization substrate. **b** Conceptual drawing of the normal and transversal characterization. **c** Conceptual drawing of the characterization system

4 Characterization

4.1 Experiment set-up for sensitivity

Sensor characterization setup is shown in Fig. 9. The sensor is pressed using a 1 nm precision displacement actuator. The actuator used was a lead zirconate titanate (PZT)-based nano-indentation system (Physik Instrumente GmbH and

Co. KG), which was mounted on the DCM 2000 micro-manipulator (Cascade Microtech, Inc.). This is a piezo-electric actuator with built-in capacitive sensor with a resolution of 1 nm. The response of the sensor is recorded at a probe station using a standard parametric analyzer (Agilent 4156A). Since the input is not the force, but the displacement, force can only be inferred by the analytical solution and finite element solution from the displacement input.

In order to characterize X–Y–Z axis, the sensor is flip chip bonded to a silicon substrate custom designed for this sensor. Gold stud bumps were made on the aluminum bondpad, and Cu–Sn stack has been plated on the mating substrate. Flip chip bonding was done using a SUSS FC150 flip chip bonder. Description of the X–Y–Z characterization method and the flip chip interface after bonding is shown in Fig. 10.

4.2 Sensitivity characterization

X–Y–Z output versus applied displacement is shown in Fig. 11. Displacement was applied up to 10 μm for each axis. Linear response is shown for all axis. Transverse sensitivity of the two affected resistors along the axis of movement showing differential signal, and resistors orthogonal to the axis of movement showing minimal change. The orthogonal axis resistors show minimal change because the two piezoresistors on each side cancel each others' change in resistance.

4.3 Stopper evaluation

We used Dage4000 multi-purpose bond tester and BS250 (ball shear, 250 gf limit) cartridge for bonding strength characterization. The measurement set up is shown in Fig. 12. The sensors were firmly attached with epoxy to a glass slide and the glass slide was held by a mechanical jig, which is a part of Dage4000. For the normal force test, the sensor was first attached to a concave silicon holder to allow vertical movement of the beams and the silicon rod. Shear force test was performed to measure the shear bonding strength with test set up shown in Fig. 12a. Normal force

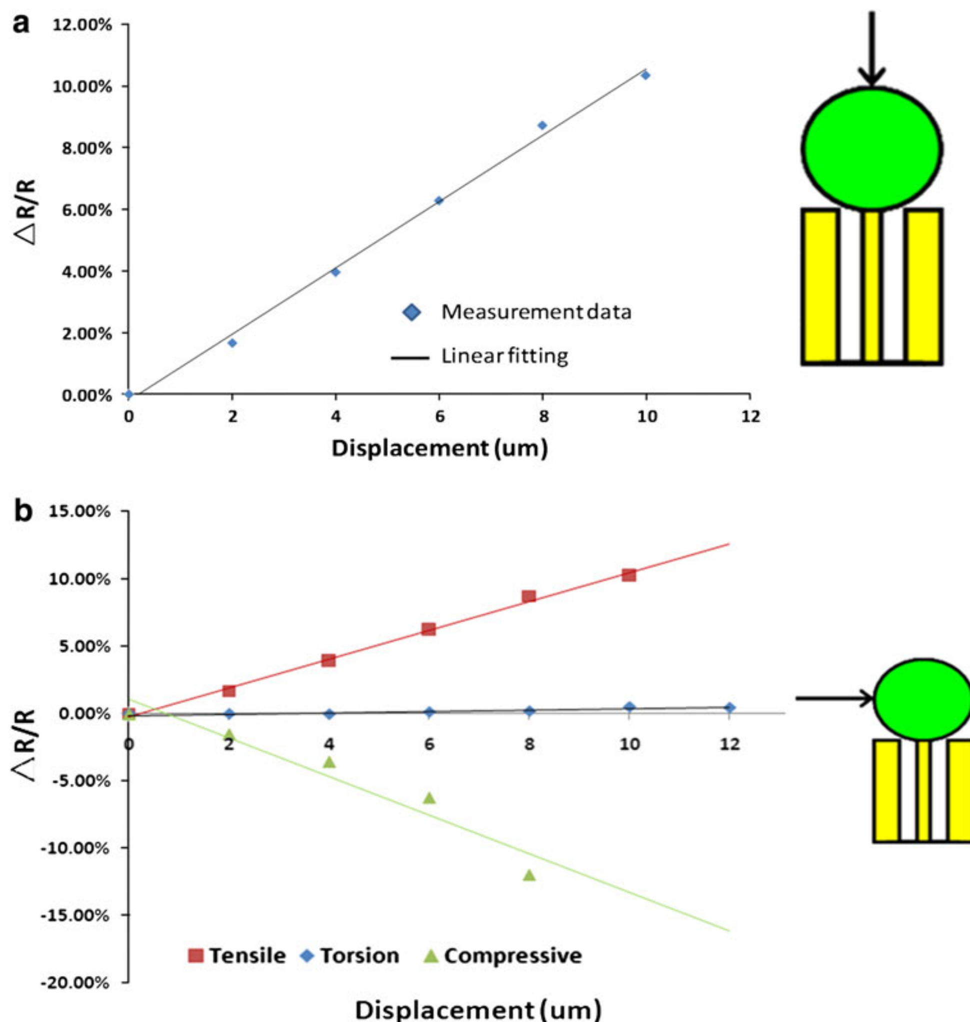

Fig. 10 **a** Sensor output versus displacement for the normal direction for one of the resistors. (nominal resistance of each resistor, *R*, is 180 kΩ), **b** transverse output of the two affected resistors along the axis of movement showing differential signal, and resistors orthogonal to the axis of movement showing minimal change

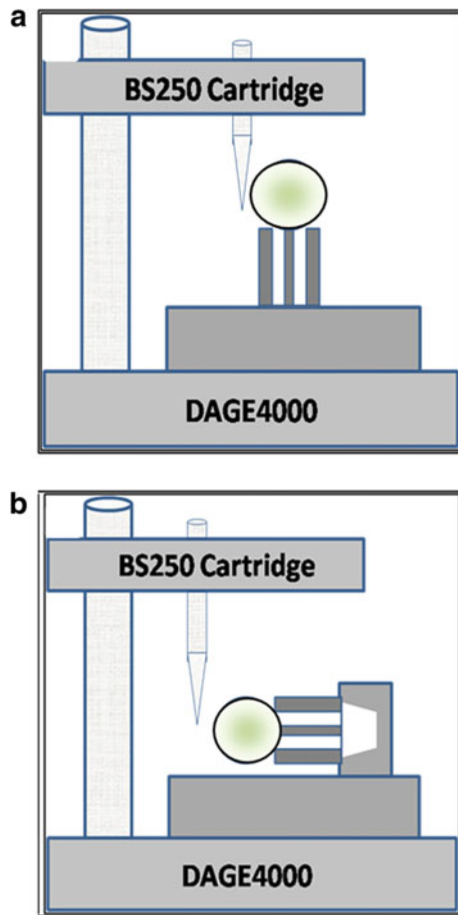

Fig. 11 Bonding strength characterization set up **a** shear force **b** normal force

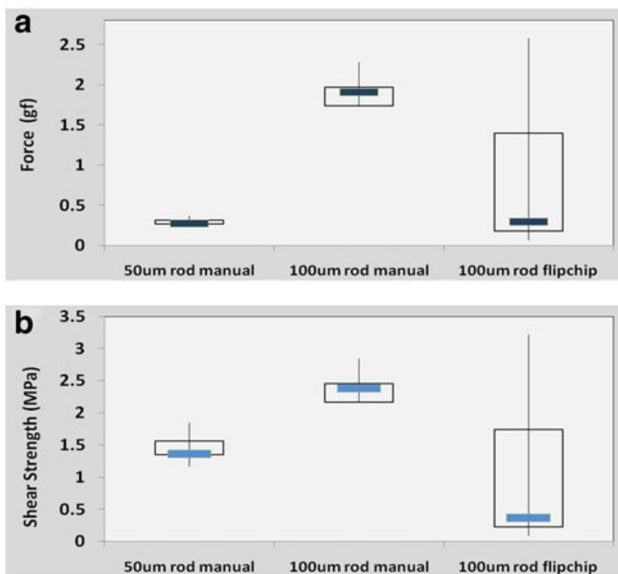

Fig. 12 Shear strength characterization result **a** in gram force **b** in Pascal (N/m^2)

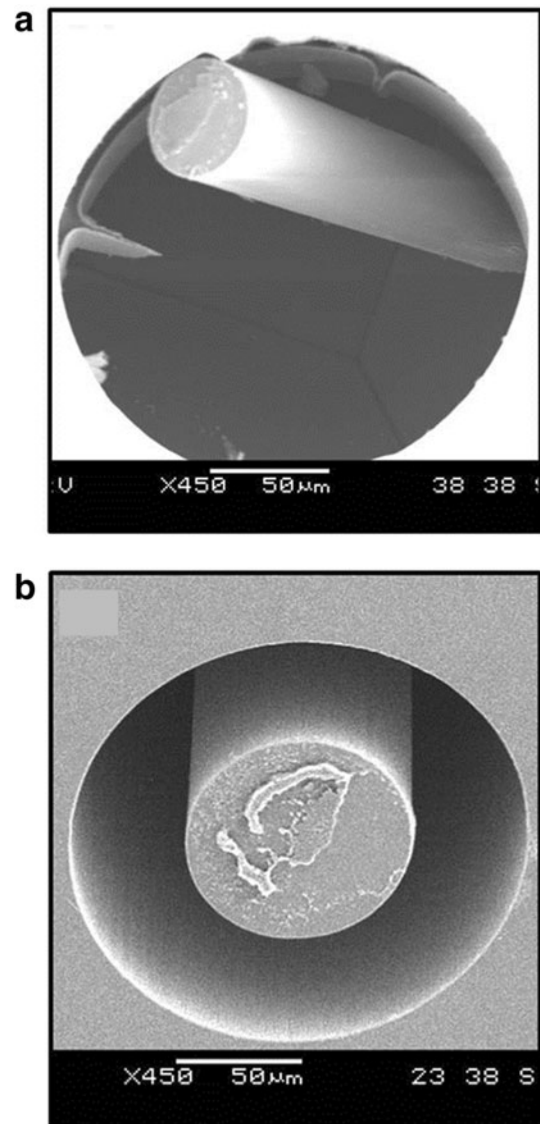

c

	50µm pillar	100µm pillar
5 - 10gf		2
10 - 15gf		1
15 - 20gf	2	
20 - 25gf	1	

Fig. 13 After normal force test **a** 50 µm rod **b** 100 µm rod. Normal test results in **c**

was tested as shown in Fig. 12b to evaluate the failure mechanism of the device under vertical force. Because this equipment was designed for shear testing, normal load testing was done in set maximum force, with increasing maximum force settings (Nondestructive mode). We started at 5 gf, with 5 gf increments.

Figure 13 shows the box-plot of shear force measurement results. Five samples for each condition of silicon rod size and bonding method prepared. Consistent results were achieved for manual bonding method, however for flip chip bonding method, the result was not consistent. Based on observation, the main cause of the inconsistent result was the stability of the ball on the holder, affecting the alignment of the bond. On the other hand, consistent result was achieved for the manual method as the whole processed was simplified. Around 2 gf for 100 μm silicon rod and 0.3 gf for 50 μm silicon rod was achieved. Converting the result into shear strength by dividing with silicon rod area, the shear bonding strength was 2.5 MPa for 100 μm silicon rod and 1.5 MPa for 50 μm silicon rod. Even though relatively high shear bonding strength was achieved, in terms of absolute load, the result was quite low for guidewire application, which has load range of 0.5–12 gf (Asahi Intecc 2010). One important finding is that the guidewire load range benchmark was obtained only from normal load, which is the most likely the main loading component in the application. Shear bonding strength here should not be a reference to gauge the guidewire reliability, but need further characterization to imitate real conditions.

For the normal force conditions, the stopper will eventually hit the rim of the force sensor, and stop (as shown in Fig. 6). But at a higher force the bond between the rod and the stopper should fail. For normal force test, only manual bonding method samples were used because only this method showed consistent shear test results. For 50 μm silicon rod, the samples under test were able to survive until 20–25 gf normal force before the mechanical stopper was broken at the base. SEM picture after normal test is shown in Fig. 13a. It is suspected that the cause of failure was overetching at the base of silicon rod which was the weakest region of the rod. 100 μm silicon rod could only achieve 10–15 gf in normal force test before the mechanical stopper was detached. However, the silicon rod was not broken as shown in Fig. 13b. Different from 50 μm silicon rod, it is suspected the failure was due to misalignment of the mechanical stopper on the silicon rod, making the force no longer perfectly aligned vertically to the silicon rod.

5 Conclusion

Herein we report a four beam tri-axial force sensor with a mechanical stopper design for tactile sensor applications in guidewire navigation. Detailed analysis on the stopper design and the relationship between the stopper sizes, the functional range of the sensor was provided. With the increase in the stopper size, the permissible displacement was reduced and hence limiting the functional range. For example, the functional range of the sensor was about 25 mN for 200 μm radius stopper and the functional range was 45 mN when the stopper radius size was reduced to 150 μm while rest of the features are kept same. The advantages of the stopper are that cantilevers will be protected from excessive deformation and also provide smooth contact to the lumen. However it is important to have good adhesion of the stopper to the silicon rod. The process improvement to increase bonding strength between mechanical stopper and silicon rod is still the focus on our ongoing research. These sensors can be further integrated with application specific integrated circuit and specialized biocompatible packaging to be used in real guidewire applications. The enhanced sensing capability in the guidewire can be used to explore new capabilities in minimal invasive surgery.

Acknowledgments This work was supported in part by A*Star science and research council under Grant 0921480070. Authors would like to thank the support from Dr. Benjamin SY Chua, and Dr. C.N. Lee of the National University of Singapore, Department of Surgery.

References

Asahi Intecc (2010) Medical products—PTCA guide wire, Web: http://www.asahi-intecc.com/medical/international/product/ptca_gw.php. Accessed 25 Sep 2010

Beccai L, Roccella S, Arena A, Valvo F, Valdastri P, Menciassi A, Carrozza MC, Dario P (2005) Design and fabrication of a hybrid silicon three-axial force sensor for biomechanical applications. Sensor Actuat A-Phys 120:370–382

Beyeler F, Muntwyler S, Nelson BJ (2009) A six-axis MEMS force-torque sensor with micro-Newton and nano-Newtonmeter resolution. J Microelectromech S 18:433–441

Bonanomi G, Rebello K, Lebouitz K, Riviere C, Di Martino E, Vorp D, Zenati MA (2003) Microelectromechanical systems for endoscopic cardiac surgery. J Thorac Cardiovasc Surg 126: 851–852

Fahlbusch, S, Fatikov S, Santa K (1998) Force sensing in microrobotic systems: an overview. In: IEEE International Conference on electronics, circuits and systems, pp 259–262

Jin WL, Mote CD (1998) Development and calibration of a sub-millimeter three-component force sensor. Sensor Actuat A-Phys 65:89–94

Neuzil P, Wong CC, Rebound J (2010a) Electrically controlled giant piezoresistance in silicon nanowires. Nano Lett 10:1248–1252

Neuzil P, Shah D, Herrera C, Jais P, Hindricks G, Natale A, Fonck E, Lambert H, Kuck KH, Reddy V Y (2010b) Does catheter contact force during RF ablation relate to AF recurrence rate? In: Proc. of Cardiostim, Nice, France, pp 176–177

Petersen KE (1998) Silicon as a mechanical material. Proc IEEE 70:420–457

Rebello KJ (2004) Applications of MEMS in surgery. Proc IEEE 92:43–55

Rowe ACH (2008) Silicon nanowires feel the pinch. Nat Nanotechnol 3:311–312

Smith CS (1954) Piezoresistance effect in germanium and silicon. Phys Rev 94:42–49

Takizawa H, Tosaka H, Ohta R, Kaneko S, and Ueda Y (1999) Development of a microfine active bending catheter equipped with MIF tactile sensors. In: Proc 12th IEEE Int. Conf. Micro Electro Mechanical Systems (MEMS'99), pp 412–417

Tibrewala A, Phataralaoha A, Buttgenbach S (2008) Analysis of full and cross-shaped boss membranes with piezoresistors in transversal strain configuration. J Micromech Microeng 18:1–6

Tonino PAL, De Bruyne B, Pijls NHJ et al (2009) Fractional flow reserve versus angiography for guiding percutaneous coronary intervention. New Engl J Med 360:213–224

Valdastri P, Harada K, Menciassi A, Beccai L, Stefanini C, Fujie M, Dario P (2006) Integration of a miniaturised triaxial force sensor in a minimally invasive surgical tool. IEEE Trans Bio-Med Eng 53:2397–2400

Valdastri P, Houston K, Menciassi A, Dario P (2007) Miniaturized cutting tool with triaxial force sensing capabilities for minimally invasive surgery. J Med Devices 1:206–211